



Original article

Fused heterocycles bearing bridgehead nitrogen as potent HIV-1 NNRTIs. Part 2: Discovery of novel [1,2,4]Triazolo[1,5-a]pyrimidines using a structure-guided core-refining approach[☆]



Liu Wang^{a,1}, Ye Tian^{a,1}, Wenmin Chen^a, Hong Liu^a, Peng Zhan^{a,*}, Dongyue Li^a, Huiqing Liu^b, Erik De Clercq^c, Christophe Pannecouque^c, Xinyong Liu^{a,*}

^a Department of Medicinal Chemistry, Key Laboratory of Chemical Biology (Ministry of Education), School of Pharmaceutical Sciences, Shandong University, 44, West Culture Road, 250012 Jinan, Shandong, PR China

^b Institute of Pharmacology, School of Medicine, Shandong University, 44, West Culture Road, 250012 Jinan, Shandong, PR China

^c Rega Institute for Medical Research, KU Leuven, Minderbroedersstraat 10, B-3000 Leuven, Belgium

ARTICLE INFO

Article history:

Received 11 January 2014

Received in revised form

28 July 2014

Accepted 29 July 2014

Available online 30 July 2014

Keywords:

DAPY

[1,2,4]Triazolo[1,5-a]pyrimidine

Bridgehead nitrogen heterocycle

anti-HIV activities

Structure–activity relationships

Molecular modeling

ABSTRACT

Guided by crystal structures of HIV-1 RT/DAPY complex and molecular modeling studies, a series of novel [1,2,4]triazolo[1,5-a]pyrimidine derivatives were rationally designed *via* structure-based core refining approach, synthesized through the readily accessible synthetic methods and evaluated for their anti-HIV activities in MT-4 cells. Preliminary biological evaluation indicated that most of the compounds exhibited marked inhibitory activity against the wild-type HIV-1 III_B. Particularly, compound **7n** was the most potent inhibitor against wild-type and K103N/Y181C double resistant mutant strain of HIV-1, possessing EC₅₀ values of 0.02 μM and 7.6 μM, respectively, which were much better than or similar to nevirapine (NVP, EC₅₀ = 0.15 μM, 2.9 μM) and delavirdine (DLV, EC₅₀ = 0.07 μM, >36 μM). Besides, some other compounds, **5b**, **7c**, **7e**, **7f**, and **7m**, were also endowed with favorable anti-HIV-1 potency (EC₅₀ = 0.07, 0.05, 0.05, 0.07, and 0.05 μM, respectively), which were better than or similar to those of NVP and DLV, suggesting a high potential to further develop this type of bridgehead nitrogen heterocycle as a novel class of NNRTIs with improved antiviral efficacy and resistance profile. The selected compound, **7i**, was found moderately inhibitory towards RT (IC₅₀ = 0.39 μM), which was higher than for ETV (IC₅₀ = 0.56 μM). Preliminary structure–activity relationships (SARs) and molecular modeling of these new analogues were detailed in this manuscript.

© 2014 Elsevier Masson SAS. All rights reserved.

1. Introduction

Human immunodeficiency virus type-1 (HIV-1) reverse transcriptase (HIV-1 RT) is a key enzyme in the HIV replicative cycle, which represents one of the main targets for the treatment of HIV/AIDS [1]. Among RT inhibitors, non-nucleoside RT inhibitors (NNRTIs) can directly inhibit RT by binding to an allosteric site,

termed as the NNRTIs binding pocket (NNIBP), which is located about 10 Å away from the RT catalytic site, [1]. HIV-1 NNRTIs are a key component of the HAART regimen for the long-term management of HIV infection because of their unique antiviral potency, high specificity and low toxicity. However, during the clinical usage of first generation NNRTIs (nevirapine, delavirdine and efavirenz), significant resistance has been generated by the emergence of mutant viral strains. Therefore, there is still need for discovery of novel HIV-1 NNRTIs with an improved potency against the wild-type (wt) and key clinically observed mutant virus strains [2–7].

The diarylpyrimidines (DAPYs) family, with two approved anti-HIV-1 drugs etravirine (ETV, Intelence[®], TMC125) and rilpivirine (Edurant[®], TMC278), has been regarded as one representative class of the promising HIV-1 NNRTIs with robust anti-HIV-1 potency against both the wt and drug-resistant strains carrying multiple mutations [6,7]. However, the pharmacokinetic profiles of most DAPY derivatives are not very satisfactory [8–10]. For example,

[☆] **Part 1:** An accompanying article: Tian Y, Du D, Rai D, Wang L, Liu H, Zhan P, De Clercq E, Pannecouque C, Liu X. Fused heterocyclic compounds bearing bridgehead nitrogen as potent HIV-1 NNRTIs. Part 1: design, synthesis and biological evaluation of novel 5,7-disubstituted pyrazolo[1,5-a]pyrimidine derivatives. *Bioorg Med Chem.* 2014; 22(7):2052–9.

* Corresponding authors.

E-mail addresses: zhanpeng1982@sdu.edu.cn (P. Zhan), xinyongl@sdu.edu.cn (X. Liu).

¹ Liu Wang and Ye Tian contributed equally to this article.

etravirine is both a substrate and an inducer of cytochrome P450 3A4 (CYP3A4), while it is an inhibitor of CYP2C9 and CYP2C19. Numerous drug–drug interactions must be considered when prescribing etravirine. Therefore, many drugs are limited on that occasion. This situation have encouraged several research groups to explore next-generation NNRTI agents with better pharmacological profiles and enhanced oral bioavailability for the treatment of HIV infections.

Based on the X-ray crystal structures of DAPYs-RT complexes and molecular modeling, the binding conformation of DAPYs resembled a horseshoe or “U” shape when bound in the NNIBP in contrast to the typical butterfly-like binding shape of the three first-generation NNRTIs. The relative flexibility of the molecules might allow DAPYs to better adapt to the plasticity of the NNIBP, which appear to be critical for maintaining potency against wt and a wide range of drug-resistant mutant HIV-1 RTs [5–7]. As shown in Fig. 1, their molecular structure consists of three rings bound by rotatable bonds with an essential NH linker between the right wing (A ring) and the central ring (B ring). The DAPYs also shared a similar pharmacophore as the first-generation NNRTIs, including hydrophobic center able to participate in π – π stacking interactions (C ring), hydrogen bond donor and acceptor. The six-membered heterocycle moiety not only stays in the center of the NNIBP, anchoring the functional groups for optimal engagement with the residues around NNIBP, but also serves as a critical hydrogen bond acceptor (the pyrimidine nitrogen at 1-position) to make hydrogen bond with the α -amino group of Lys101. Besides, the NH linker connecting the central B ring and the right A wing can function as a hydrogen bond donor able to interact with the backbone carbonyl of Lys101 [5–7]. These conclusions provided critical insights for further structural evolution or scaffold refining towards improving their activity and drug resistance profiles.

Scaffold refining *via* the replacement of the central core in bioactive molecules combined with introducing privileged substituents is a common practice in contemporary medicinal

chemistry to obtain intellectual property and novel hits, as well as to improve synthetic accessibility [6]. To discover highly potent DAPY derivatives with better drug-like properties that are easier to synthesize or to avoid existing patent art, further modifications were focused on the replacement of the pyrimidine core with an array of aromatic scaffolds [11].

In this regard, previous research in our laboratory using structure-based drug design and isosteric principle resulted in the discovery of a novel series of potent DAPYs back-up analogues, such as pyridazines (**DL-8g**), nitropyridines (**JW-7a2**), and pyrimidines (**XL-7a**), as RT inhibitors which proved to be highly effective in inhibiting HIV-1 replication at low or double-digit nanomolar concentrations [12–14]. According to the molecular modeling and structure–activity relationship (SAR) results, the central pyrimidine ring of DAPYs is relatively tolerant.

Recently, a closely related scaffold type, pyrrolopyrimidine, has been successfully investigated for the discovery of highly potent NNRTIs against wild-type and single mutant strains. Especially, RDEA427 (preclinical) and RDEA640 (Fig. 1) are superior to efavirenz against a batch of NNRTI-resistant strains and show weaker binding affinity to serum proteins than rilpivirine and efavirenz. RDEA640 and RDEA427 also demonstrate a low potential for human cytochrome P450 induction and a low cytotoxicity. The favorable *in vitro* pharmacology profiles of these novel molecules display great potential for improved performance over the existing NNRTIs and warrants further clinical evaluation [15].

Additionally, Riley et al. studied CYP3A4 inhibition of drugs that contained pyridine and suggested general rules for reducing this inhibition of nitrogen heterocycle-containing drugs [16]. They concluded that the decreased lipophilicity (LogD) of the molecule and increased steric hindrance to the heterocycle (which reduced the interaction of the nitrogen lone pair with the 3A4 heme group) were beneficial to reduce CYP3A4 inhibition. Other structure–metabolism relationship studies have shown that incorporation of one or more nitrogen atoms in the rings decreases the electron

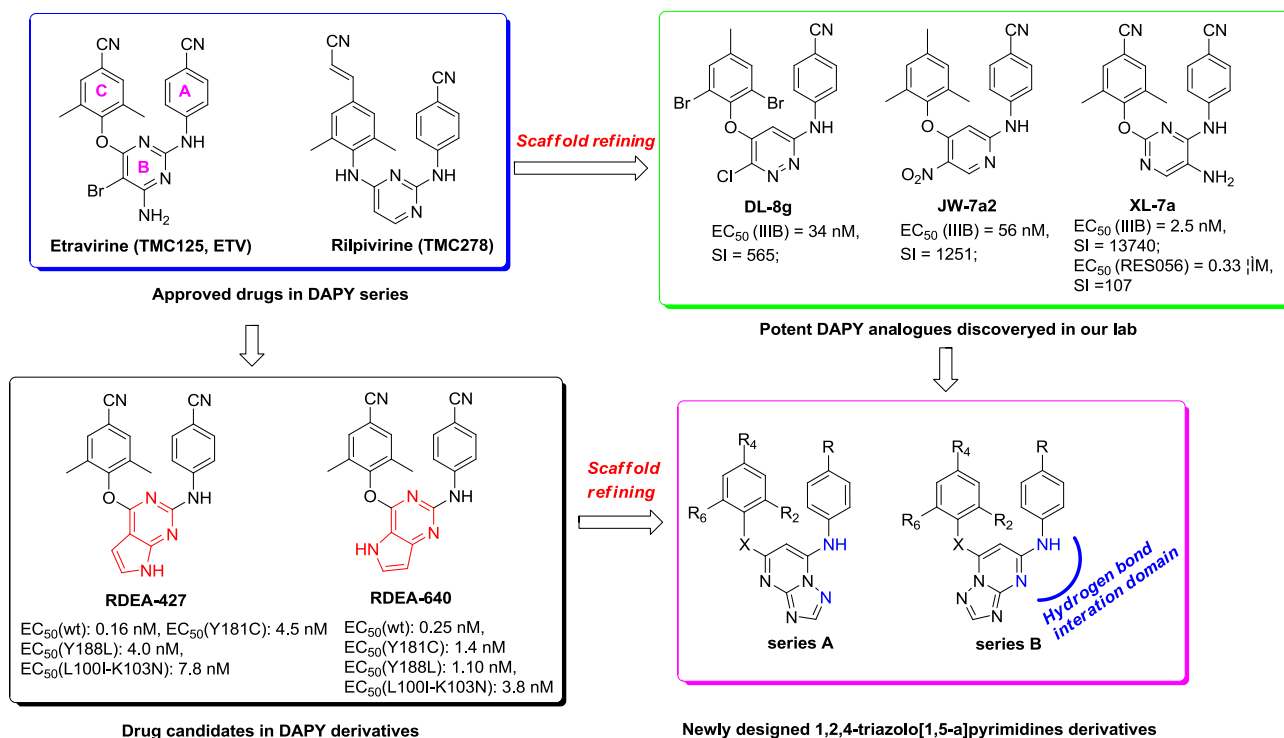


Fig. 1. Design of 1,2,4-triazolo[1,5-a]pyrimidine derivatives as DAPYs back-up series *via* a scaffold (core) refining approach.

density on the carbons of aromatic ring, thereby decreasing P450-mediated interaction [17]. Thus, the lower reactive rings with multiple nitrogens improve the metabolic properties of these prime molecules.

As an extension of our investigations and with the aim to generate novel NNRTIs with desirable potency and properties, we focused on our interests on the bridgehead nitrogen heterocycles, which were considered as privileged structures in numerous biologically active compounds [17,18] (including drugs, like Zaleplon, Zolpidem and Temozolomide) and conformed to the optimizing strategies for better metabolic mentioned above. Therefore, a novel series of 1,2,4-triazolo[1,5-a]pyrimidine derivatives were designed based on the fused pyrrolopyrimidine series as the lead. In these structures the pyrimidine ring in the original DAPY scaffold was replaced with a synthetically accessible 1,2,4-triazolo[1,5-a]pyrimidine heterocycle to ensure the optimal pharmacodynamic and pharmacokinetic properties, while the NH linker connecting the central ring and the right wing, and the privileged substitutions of A and C rings were maintained in view of their paramount importance in the previous series. Further, we substituted the A and C rings with additional groups to investigate their influence on the HIV inhibitory activity. General structure of such a new scaffold is illustrated in Fig. 1.

Herein, we will further report the synthesis, anti-HIV evaluation of [1,2,4]triazolo[1,5-a]pyrimidine derivatives against wt HIV-1 and HIV-2 ROD, as well as against a double-mutated HIV-1 strain RES056 (K103N + Y181C). In addition, preliminary SAR data and molecular modeling results of these new compounds are also discussed to provide deeper insight into their interactions with the allosteric binding site.

2. Results and discussion

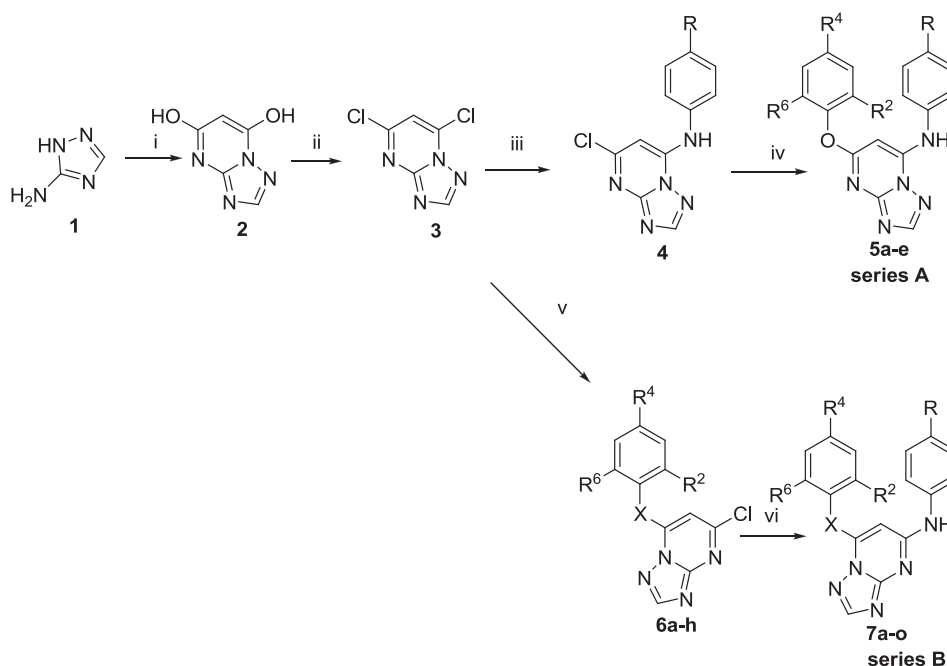
2.1. Chemistry

To achieve the synthesis of the target compounds **5(a–e)** and **7(a–o)**, the steps outlined in Scheme 1 were adopted. The

straightforward synthetic procedures are described in the experimental section. Briefly, the commercially available material 2H-1,2,4-triazol-3-amine (**1**) was condensed with the diethyl malonate to form the [1,2,4]triazolo[1,5-a]pyrimidine-5,7-diol (**2**) [19–21]. Chlorination with phosphorous oxychloride gave the 5,7-dichloro-[1,2,4]triazolo[1,5-a]pyrimidine (**3**) [19–21]. Then the 7-Cl of compound **3** underwent a facile nucleophilic aromatic substitution reaction with 4-aminobenzonitrile in ethanol to afford 4-(5-chloro-[1,2,4]triazolo[1,5-a]pyrimidin-7-ylamino)benzotrile (**4**) exclusively [21–23]. Treatment of intermediate **4** with a range of substituted phenols and potassium carbonate under 85 °C in DMF gave the target compounds 4-(5-substituted phenoxy-[1,2,4]triazolo[1,5-a]pyrimidin-7-ylamino)benzotriles (series **5**). Alternatively, replacement of the 7-chloro of compound **3** with the corresponding ArOH (for compounds N-(4-substituted-phenyl)-7-substituted phenoxy-[1,2,4]triazolo[1,5-a]pyrimidin-5-amines) or a ArNH₂ (for compounds N⁵-(4-substituted-phenyl)-N⁷-substituted-phenyl-[1,2,4]triazolo[1,5-a]pyrimidine-5,7-diamines), in the presence of potassium carbonate in DMF, yielded the desired intermediates **6(a–h)** [21–23]. Compounds **7a–o** were prepared by further treatment of compounds **6(a–h)** with the required amines. The newly synthesized compounds were characterized by physicochemical and spectral means and both analytical and spectral data of all the compounds were found to be in full agreement with the proposed structures.

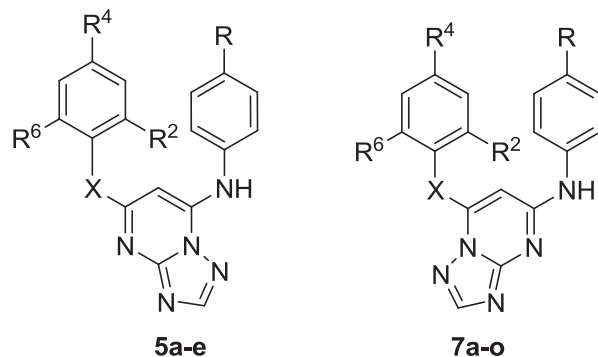
2.2. Anti-HIV evaluation

All of the newly synthesized [1,2,4]triazolo[1,5-a]pyrimidines derivatives together with the marketed drugs of NVP and DLV as the controls were evaluated for their anti-HIV activity (against the wt HIV-1 strain III_B [24], the commonly encountered double mutant strain RES056 (K103N + Y181C) and HIV-2 strain ROD [25,26]) and cytotoxicity in MT-4 cells. The methodology of the anti-HIV assay has been previously described [27,28]. The results, expressed as EC₅₀ (anti-HIV activity), CC₅₀ (cytotoxicity) and SI (selectivity index, given by the CC₅₀/EC₅₀ ratio), are summarized in Table 1. The



Scheme 1. Synthetic route to [1,2,4]triazolo[1,5-a]pyrimidine derivatives. Reagents and conditions: (i) Diethyl malonate, Na, EtOH, reflux; (ii) POCl₃, 95 °C; (iii) ArNH₂, EtOH, rt; (iv) ArOH, K₂CO₃, DMF, 85 °C; (v) ArOH or ArNH₂, K₂CO₃, DMF, 30 °C; (vi) ArNH₂, 150–160 °C.

Table 1
HIV inhibitory effect^a and cytotoxicity of the title compounds.



Compd	R ² = R ⁶	R ⁴	R	X	EC ₅₀ (μM) ^b			CC ₅₀ (μM) ^c	SI ^d		
					III _B	RES056	ROD		III _B	RES056	ROD
5a	Me	H	CN	O	1.5 ± 1.0	>253	>253	253 ± 33	170	<1	<1
5b	Me	Me	CN	O	0.07 ± 0.06	≥50	>106	106 ± 46	1449	≤2	<1
5c	Me	Br	CN	O	0.30 ± 0.09	>128	>128	128 ± 36	427	<1	<1
5d	Cl	Cl	CN	O	0.30 ± 0.09	>32	>32	32 ± 2.0	109	<1	<1
5e	F	F	CN	O	>174	>174	>174	174 ± 19	<1	<1	<1
7a	Me	H	CN	O	1.3 ± 0.8	>233	>233	233 ± 2.4	182	<1	<1
7b	Cl	H	CN	O	3.4 ± 2.4	>150	>150	150 ± 41	44	<1	<1
7c	Me	Me	CN	O	0.05 ± 0.04	>164	>164	164 ± 63	3198	<1	<1
7d	Me	Me	NO ₂	O	0.6 ± 0.5	>33	>33	33 ± 1.7	57	<1	<1
7e	Me	Me	Cl	O	0.05 ± 0.02	>46	>46	46 ± 5.5	864	<1	<1
7f	Me	Me	Me	O	0.07 ± 0.02	>47	>47	47 ± 2.3	649	<1	<1
7g	Me	Me	OMe	O	0.2 ± 0.1	>37	>37	37 ± 31	165	<1	<1
7h	Me	Br	CN	O	0.23 ± 0.07	>136	>136	136 ± 31	579	<1	<1
7i	Me	CN	CN	O	1.2 ± 0.8	>224	>224	224 ± 22	182	<1	<1
7j	Me	Cl	CN	O	0.4 ± 0.3	>104	>104	104 ± 32	256	<1	<1
7k	Cl	Cl	CN	O	0.6 ± 0.3	>29	>29	29 ± 2.8	47	<1	<1
7l	Br	Br	CN	O	0.3 ± 0.2	>47	>47	47 ± 24	142	<1	<1
7m	Br	Me	CN	O	0.05 ± 0.01	>192	>192	192 ± 34	3618	<1	<1
7n	Me	Me	CN	NH	0.02 ± 0.01	7.6 ± 0.4	>190	190 ± 5.7	8986	25	<1
7o	Me	H	CN	NH	2.1 ± 3.3	>272	>272	272 ± 44	127	<1	<1
NVP	–	–	–	–	0.15 ± 0.08	2.9 ± 1.8	–	>15	>14	>5	–
DLV	–	–	–	–	0.07 ± 0.05	>36	–	>36	>494	X1	–
ETV [23]^e	–	–	–	–	0.003 ± 0.0002	0.026 ± 0.004	–	>4.6	>1537	>177	–

^a All of the title compounds were evaluated for their anti-HIV activity against the wt HIV-1 strain III_B, the commonly encountered double mutant strain RES056 (K103N + Y181C) and HIV-2 strain ROD.

^b EC₅₀: concentration of compound required to achieve 50% protection of MT-4 cells against HIV-1-induced cytopathic effect, as determined by the MTT method.

^c CC₅₀: concentration required to reduce the viability of mock-infected cells by 50%, as determined by the MTT method.

^d SI: selectivity index (CC₅₀/EC₅₀), and the SI values: X1 stands for ≥1 or <1.

^e Data were obtained from the same lab of the Rega Institute for Medical Research, KU Leuven, Belgium.

activities of etravirine (ETV) were also included as reference materials [29].

As seen from Table 1, the results indicated that the majority of target compounds have displayed remarkable potency against wt HIV-1 (III_B) with EC₅₀ values between 0.02 μM and 3.4 μM, except for compound **5e** (EC₅₀ > 174 μM). Most of them are of low toxicity in MT-4 cells with CC₅₀ values more than 100 μM. Encouragingly, the most effective compound **7n** with an EC₅₀ of 0.02 μM against wild-type HIV-1, was better than nevirapine (0.15 μM) and DLV (0.07 μM), but it was inferior to the clinically used etravirine (0.003 μM) [29]. Moreover, **7n** exhibited an excellent selectivity index (SI against the wild-type HIV-1 was approximately 9000). Besides, five other compounds, **5b** (EC₅₀ = 0.07 μM, SI = 1449), **7c** (EC₅₀ = 0.05 μM, SI = 3198), **7e** (EC₅₀ = 0.05 μM, SI = 864), **7f** (EC₅₀ = 0.07 μM, SI = 649) and **7m** (EC₅₀ = 0.05 μM, SI = 3618), were more active than reference drugs NVP and DLV against wt HIV-1 (III_B). These promising results demonstrated that the isosteric replacement of [1,2,4]triazolo[1,5-a]pyrimidine for pyrimidine in the central B-ring of DAPY compounds was gratifying and afforded a series of potent [1,2,4]triazolo[1,5-a]pyrimidine NNRTIs.

Based on the results of antiviral assay (Table 1), several important structural features for conferring optimum HIV inhibition and cytotoxicity were investigated and summarized as the following:

The data clearly demonstrated that the orientation of the central [1,2,4]triazolo[1,5-a]pyrimidine ring does not significantly affect the anti-HIV potency by comparing the activities of the counterparts between series **5** and **7** (**5a** vs **7a**; **5b** vs **7c**; **5c** vs **7h**; **5d** vs **7k**), indicating that the [1,2,4]triazolo[1,5-a]pyrimidine provided similar conformational and electronic contributions to the binding of the inhibitors with the NNIBP in both series.

Next we turned our attention to SAR of the left ring in **5** series. In the case of 2,6-dimethylphenoxy analogues (**5a**, **5b**, **5c**), a clear order of R⁴-substitution for anti-HIV activity was observed by direct comparison: CH₃ (**5a**) > Br (**5c**) > H (**5b**). In the case of 2,4,6-trisubstituted-phenoxy derivatives (**5b**, **5d**, **5e**), we found the antiviral potency in the order of 2,4,6-trimethyl > 2,4,6-trichloro > 2,4,6-trifluoro.

As highlighted in Table 1, the potency of **7** series is also strongly dependent on the nature of substituents at the R⁴ position of the C-ring. In the case of the 2,6-dimethylphenoxy analogues with

R = CN, the order of R⁴-substitution for anti-HIV activity ranked as follows: CH₃ (**7c**) >> Br (**7h**) > Cl (**7j**) > CN (**7i**) > H (**7a**), which is similar to that of the **5** series. This conclusion is in agreement with the observation in 2,6-dichlorophenoxy analogues (Cl > H) and 2,6-dibromophenoxy analogues (CH₃ > Br). These results seemed to indicate that R⁴ substituents with appropriate bulk are beneficial for potency.

Comparatively speaking, the anti-HIV-1 activity has been less affected by the nature of the substituents at the R²/R⁶ position than at R⁴. Bearing the identical R⁴-CN substituent, the R²/R⁶-methyl derivative **7c** and R²/R⁶-bromo derivative **7m** shared the same anti-HIV activity (EC₅₀ = 0.05 ± 0.04 μM, EC₅₀ = 0.05 ± 0.01 μM, respectively). Moreover, the R²/R⁶-methyl derivative **7j** showed activity in the low submicromolecular range with an EC₅₀ value (0.4 μM) comparable to that of the R²/R⁶-chloro derivative **7k** (EC₅₀ = 0.6 μM). The substituents ranked as 2,4,6-trimethyl >> 2,4,6-tribromo > 2,4,6-trichloro for 2,4,6-trisubstituted-phenoxy derivatives (**7c**, **7l**, **7k**) in the order of antiviral potency.

Regarding to SAR of the R substituent at the *para* position of the A-ring, a declining trend of anti-HIV-1 (III_B) potency was found for the congeners with the 2,4,6-trimethylphenoxy group: **7c** (CN) > **7e** (Cl) > **7f** (Me) > **7g** (OMe) > **7d** (NO₂). The R-cyano compound **7c** also showed the best toxicity profile. This implies that the *para*-cyano moiety could be preferred for anti-HIV activity.

Furthermore, the replacement of the O linker connecting the central B ring and the left C wing of **7c** with NH linker culminated in the identification of the most potent compound **7n**. But this improvement did not appear in the case of **7a** and **7o**.

Like for other typical NNRTIs, all the title compounds were inactive against the HIV-2 strain. However, compound **7n** possessed potent activity against HIV-1 mutated strain RES056 bearing both K103N and Y181C mutations in MT-4 cells with an EC₅₀ value of 7.6 μM, which was lower than that for DLV (EC₅₀ > 63 μM). Although compound **7n** was still less potent than NVP (EC₅₀ = 2.9 μM) and ETV (EC₅₀ = 0.026 μM), it is a good starting point for further modifications.

2.3. Inhibition of HIV-1 RT

With the aim to further confirm the drug target of [1,2,4]triazolo [1,5-a]pyrimidine derivatives, the selected title compound **7i** (due to the high degree of structural similarity with ETV) was tested in enzymatic assays against highly purified recombinant HIV-1 RT which use poly [A] × oligo [dT]₁₅ as template/primer and digoxigenin-/biotin-labeled dUTP as nucleotides in this assay [30,31]. The detection and quantification of the synthesized DNA represented the activity of HIV-1 RT. IC₅₀ values correspond to the concentration of the [1,2,4]triazolo[1,5-a]pyrimidine derivatives required to inhibit biotin-dUTP incorporation by HIV-1 RT by 50%. As shown in Table 2, compound **7i** exhibited moderate inhibition of enzymatic activity with an IC₅₀ value of 0.39 μM, which was slightly lower than that of ETV (0.56 μM). The results show that these newly synthesized derivatives, represented by compound **7i**, are targeted at HIV-1 RT, thus acting as genuine NNRTIs.

Table 2
Inhibitory activity of compound **7i** against HIV-1 RT.

Compd.	7i	Etravirine
IC ₅₀ (μM) ^a	0.39	0.56

^a 50% inhibitory concentration of tested compounds required to inhibit biotin deoxyuridine triphosphate (biotin-dUTP) incorporation into the HIV-1 (wt) RT by 50%.

2.4. Molecular modeling analysis

To understand the interactions between these inhibitors and the target, the representative compounds **5b**, **7c**, **7i**, **7n** along with the reference compounds ETV, RDEA427 and RDEA640 were docked into the NNIBP of HIV-1 RT by Surflex-Dock module of Sybyl-X 1.1 software. X-ray crystal structure of HIV-1 wt RT (PDB code: 3MEC) and K103N/Y181C mutant RT (PDB code: 3BGR) were used as the input structures for docking calculations. Default parameters were used as described in the Sybyl-1.1 manual unless otherwise specified. The theoretical binding modes of these compounds to the NNIBP are shown in Fig. 2.

It is important to point out that the synthesized compounds adopted a very similar conformation of interaction in the NNIBP as that of the reference DAPY compound ETV. As illustrated in Fig. 2a–c, the common left wing of compounds **5b**, **7c** and **7n** fits into the aromatic-rich binding pocket, surrounded by the aromatic side chains of Tyr188, Tyr181, Phe227, and Trp229. And right wing in the pocket lined by Lys103, Val106, Leu234, Pro236 and Tyr318. These compounds undergo one or two hydrogen bonds with the backbone of residue Lys101 through the NH linker moiety with the right wing or the nitrogen atom of the central ring, which is important for the affinity between inhibitor and RT. Besides, the fusing triazole part of the [1,2,4]triazolo[1,5-a]pyrimidine could enhance the van der Waals interactions (for **7c** and **7n**) or the hydrogen bonds (for **5b**) between the inhibitors and the adjacent amino acid residues (Glu138, Val179, and Lys101) within the binding pocket of RT, explaining the observed nearly equal potency against wt HIV-1 between **5a–e** and their counterparts in the **7** series. All the above interactions would favor the high binding affinity and increased antiviral activity.

Detailed analysis of the superimposed binding modes of **7n** (purple) and ETV (pink) in the HIV-1 RT showed that the fused triazole part of the [1,2,4]triazolo[1,5-a]pyrimidine overlays with the amino and bromine groups of ETV. Although the established hydrogen bond between ETV and Glu138 was not observed in **7n**, the fused triazole part could interact favorably with the Glu138 side chain, giving rise to compensatory van der Waals interactions, which may explain that the representative compound **7i** exhibited similar activities with ETV against the wt RT.

Compound **7n** was also simulated with a K103N/Y181C mutant RT binding pocket (PDB code: 3BGR). It is worth noting that this mode of binding of **7n** allows to keep the conformational flexibility, which may compensate for the effects of resistance mutations. Secondly, the result revealed that the potent compound retained the hydrogen bond between NH and Asn103. This observation is in agreement with the conclusion that the potent compounds are able to accommodate themselves in the mutant binding pocket so as to retain the key hydrogen bond and efficacy against HIV-1 mutant strains.

To further study the reason why the designed compounds are less active than pyrrolopyrimidine series, comparison between these compounds for their binding conformations and docking scores were conducted. As shown in Fig. 2e–f, the designed compounds share a closely similar conformation with RDEA427 and RDEA640 both in wild and mutant RT. Then obtained docking scores presented in Tables 3 and 4 display more detailed information. All these compounds have excellent total scores. Although the scores are not completely consistent with the biological assay, the results reflect the difference between designed compounds and the reference to a certain extent. Most of the figures of the tested compounds and reference molecules are very close, while the absolute values of the 'Crash' item of **5b**, **7c**, **7i** and **7n** are significantly larger than these of the RDEA427 and RDEA640. This indicates that the larger degree of inappropriate penetration by the designed

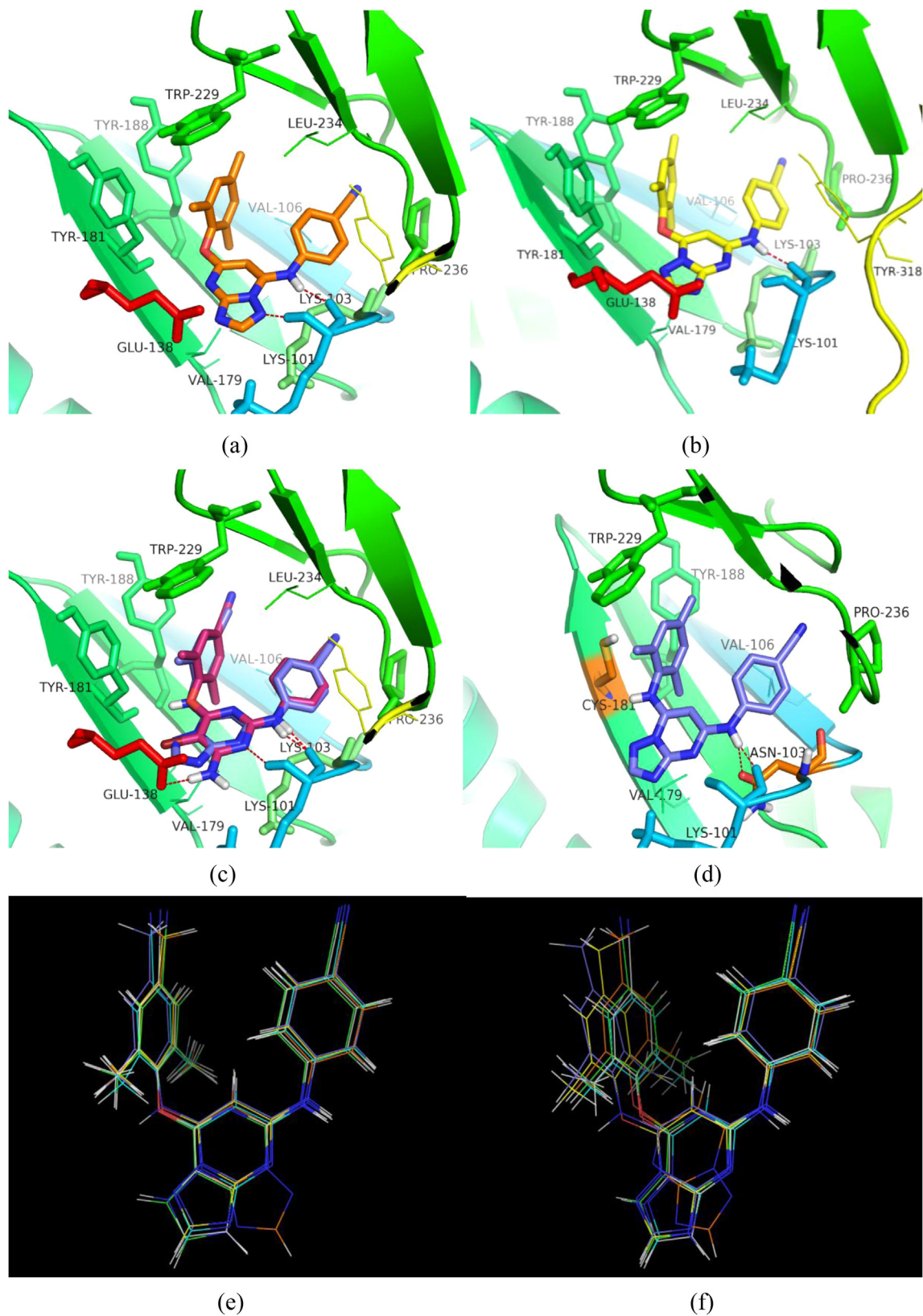


Fig. 2. (a) Predicted binding mode of compound **5b** in the allosteric site of HIV-1 wt RT (PDB code: 3MEC); (b) Predicted binding mode of compound **7c** in the allosteric site of HIV-1 wt RT (PDB code: 3MEC); (c) Superimposition of the docked conformations of **7n** (purple) and **ETV** (pink) in the HIV-1 RT (PDB code: 3MEC); (d) Predicted binding mode of compound **7n** in the allosteric site of HIV-1 K103N/Y181C mutant RT (PDB code: 3BGR). The docking results are shown by PyMOL. Hydrogen bonds are indicated by dashed lines; (e) & (f) Molecular superposition of **5b** (orange), **7c** (yellow), **7i** (cyan), **7n** (purple), RDEA427 (green), and RDEA640 (white) in the binding site of 3MEC and 3BGR, respectively. (For interpretation of the references to colour in this figure legend, the reader is referred to the web version of this article.)

Table 3
Docking scores^a of **5b**, **7c**, **7i**, **7n**, RDEA427 and RDEA640 binding into wild RT (3MEC).

Comp.	T_S	C	P	S	D_S	P_S	G_S	CHS	CS	G_C
RDEA640	10.25	-1.29	1.38	0.80	-175.78	-99.34	-328.79	-40.41	5	5
RDEA427	9.94	-1.35	1.36	0.89	-177.54	-94.16	-322.15	-38.68	5	5
5b	8.95	-2.39	1.86	0.79	-157.88	-90.44	-323.56	-42.04	5	5
7c	8.87	-2.16	1.30	0.81	-167.00	-92.09	-321.22	-38.97	5	5
7n	8.71	-2.49	1.28	0.78	-169.37	-89.17	-316.94	-42.73	5	5
7i	8.69	-1.93	1.32	0.85	-167.94	-86.01	-320.96	-36.12	5	5

^a T_S = Total_score; C = Crash; P = Polar; S = Similarity; D_S = D_SCORE; P_S = PMF_SCORE; G_S = G_SCORE; CHS = CHEMSCORE, CS = CSCORE, G_S = GLOBAL_CSCOR.

molecules into the RT and of interpenetration (self-clash) between ligand atoms that are separated by rotatable bonds might explain why this novel series demonstrated relatively lower anti-HIV-1 activity. These findings provide valuable information for the rational design of effective inhibitors with better therapeutic profiles for the treatment of AIDS.

3. Conclusions

In this article, based on the structure-based core-refining design, replacement of the heterocycle fragment in the previously reported DAPYs lead structures with a bridgehead nitrogen 1,2,4-triazolo[1,5-a]pyrimidine heterocycle led to the discovery of a novel series of potent NNRTIs. Most of these new congeners exhibited moderate to excellent activity against wild-type virus with an EC₅₀ value ranging from 3.41 μM to 0.02 μM. Preliminary SAR was established. Among the newly synthesized compounds, **7n** was identified as the most active compound (EC₅₀ = 0.02 μM, SI = 8986) associated with moderate activity against the HIV-1 double mutant strain (K103N + Y181C) with an EC₅₀ value in 7.61 μM, suggesting a high potential to further develop these compounds as a novel class of NNRTIs with improved antiviral efficacy and resistance profile. None of the compounds exhibited activity against the HIV-2 ROD strain. Furthermore, the selected 1,2,4-triazolo[1,5-a]pyrimidine **7i** showed moderate activity against wt RT. Molecular modeling studies with representative compounds were performed to gain insight into its binding mode with the allosteric site of HIV-1 RT, and to provide the basis for further structure-guided design of new NNRTIs candidates. Ongoing studies involve extension of the illustrated SAR clues to identify additional activity parameters in the bridgehead nitrogen heterocycle scaffold to overcome drug-viral resistance.

4. Experimental section

4.1. Chemistry

All melting points were determined on a micromelting point apparatus and are uncorrected. Infrared spectra (IR) were recorded with a Nexus 470FT-IR Spectrometer. ¹H NMR spectra were obtained on a Bruker Avance-600 NMR-spectrometer in the indicated solvents. Chemical shifts are expressed in δ units and TMS as internal reference. Mass spectra were taken on an LC Autosampler Device:

Standard G1313A instrument. TLC was performed on silica gel GF254 for TLC (Merck) and spots were visualized by iodine vapors or by irradiation with UV light (254 nm). Flash column chromatography was performed on a column packed with silica gel 60 (230–400 mesh). Solvents were reagent grade and, when necessary, were purified and dried by standard methods. Concentration of the reaction solutions involved the use of rotary evaporator at reduced pressure.

4.1.1. General procedure for the synthesis of 5,7-dichloro-[1,2,4]triazolo[1,5-a]pyrimidine (**3**)

A mixture of 1*H*-1,2,4-triazol-5-amine (**1**) (5.0 g, 59.5 mmol), diethyl malonate (9.52 g, 59.5 mmol), and sodium ethoxide (4.05 g, 59.5 mmol) was heated under reflux in absolute ethanol (50 mL) for 12 h. After removal of the solvent, the residue was poured into ice water, and extracted with ethyl acetate for 3 times. The water layer was separated, the pH of liquid was adjusted to 1.0 with concentrated hydrochloric acid. After cooling in ice water, white solid was formed, filtered, washed with water, and dried under vacuum to give [1,2,4]triazolo[1,5-a]pyrimidine-5,7-diol (**2**) 5.8 g with 65–70% yield. Mp: 238–240 °C. ESI-MS: *m/z* 151.1 (M–1); C₅H₄N₄O₂ (152.0334).

Compound 5,7-dichloro-[1,2,4]triazolo[1,5-a]pyrimidine (**3**) was synthesized as previously described. Concretely, compound [1,2,4]triazolo[1,5-a]pyrimidine-5,7-diol (**2**) 6.08 g (40 mmol) was added to 57 mL (600 mmol) of phosphorous oxychloride and heated under reflux for 12 h in a round bottom flask, during which the solid dissolved and hydrogen chloride was evolved. Excess phosphorous oxychloride was removed by distillation at reduced pressure in a steam-bath and the residue triturated with ice water. The mixture was extracted with methylene chloride. Then the organic layer was separated, washed with water, dried over anhydrous sodium sulfate, filtered and concentrated to give the crude product 5,7-dichloro-[1,2,4]triazolo[1,5-a]pyrimidine (**3**) as yellow solid, 4.2 g, Yield: 50–60%. mp: 126–130 °C. ESI-MS: *m/z* 189.4(M+1), 191.3(M+3), 193.3(M+5); C₅H₂Cl₂N₄ (187.9657). Compound **3** was used in the next step without further purification.

4.1.2. General procedure for the synthesis of 4-(5-substituted phenoxy-[1,2,4]triazolo[1,5-a]pyrimidin-7-ylamino) benzonitriles (**5a–e**)

The 4-aminobenzonitrile (1.56 g, 13.2 mmol) was added to 5,7-dichloro-[1,2,4]triazolo[1,5-a]pyrimidine (**3**) (2.5 g, 13.2 mmol) in

Table 4
Docking scores of **5b**, **7c**, **7i**, **7n**, RDEA427 and RDEA640 binding into mutant RT (3BGR).

Comp.	T_S	C	P	S	D_S	P_S	G_S	CHS	CS	G_C
RDEA640	10.38	-0.85	1.86	0.65	-160.93	-81.75	-305.52	-36.76	5	5
RDEA427	10.21	-0.66	1.70	0.64	-161.36	-86.20	-301.19	-34.59	5	5
5b	10.03	-1.17	2.13	0.69	-159.08	-83.68	-293.76	-38.46	5	5
7i	9.74	-0.97	1.77	0.66	-164.92	-66.78	-298.22	-31.93	5	5
7c	9.38	-0.70	1.59	0.70	-158.51	-90.47	-282.52	-34.80	5	5
7n	8.46	-1.14	1.51	0.76	-163.88	-97.48	-282.91	-39.10	5	5

absolute ethanol (35 mL) and stirred at room temperature for 6 h. The reaction mixture was filtered, washed with cold ethanol, and dried under vacuum to give the crude product 4-((7-chloro-[1,2,4]triazolo[1,5-*a*]pyrimidin-5-yl)amino)benzotrile (**4**) as white solid. 3.3 g, yield: 92%. ESI-MS: *m/z* 271.4(M+1), 273.4(M+3); C₁₂H₇ClN₆ (270.0421).

The appropriate substituted phenols (1.2 equiv.) were dissolved in anhydrous DMF (10 mL) in the presence of anhydrous K₂CO₃ (1 equiv.) at room temperature followed by addition of crude intermediate **4** (1.0 equiv.). The reaction mixture was stirred at 150 °C for 8–12 h (monitored by TLC). The solvent was cooled to room temperature, and some water was added. The residue was extracted with ethyl acetate for several times, and the combined organic phase was washed with water, and dried over anhydrous sodium sulfate to give the corresponding crude products, which were purified by flash column chromatography (ethyl acetate: petroleum ether = 1:2) to afford five target compounds **5a–e**, respectively. Yields ranged from 5 to 10%.

4.1.2.1. 4-(5-(2,6-Dimethylphenoxy)-[1,2,4]triazolo[1,5-*a*]pyrimidin-7-ylamino)benzotrile (**5a**). White solid, yield 10%. mp: 298–300 °C. ¹H NMR (DMSO-*d*₆, 400 MHz) δ: 10.15 (s, 1H, NH), 8.43 (s, 1H, triazole-H), 7.97 (d, 2H, *J* = 8.8 Hz, Ph-H), 7.81 (d, 2H, *J* = 8.8 Hz, Ph-H), 7.32 (m, 3H, OPh-H), 5.68 (s, 1H, pyrimidine-H), 2.18 (s, 6H, CH₃). IR (KBr, cm⁻¹): 3303 (NH), 2223 (CN). ESI-MS: *m/z* 357.4 (M+1); C₂₀H₁₆N₆O (356.1386).

4.1.2.2. 4-(5-(Mesityloxy)-[1,2,4]triazolo[1,5-*a*]pyrimidin-7-ylamino)benzotrile (**5b**). White solid, yield 10%. ¹H NMR (DMSO-*d*₆, 400 MHz) δ: 10.14 (s, 1H, NH), 8.43 (s, 1H, triazole-H), 7.98 (d, 2H, *J* = 8.8 Hz, Ph-H), 7.81 (d, 2H, *J* = 8.8 Hz, Ph-H), 7.12 (s, 2H, OPh-H), 5.70 (s, 1H, pyrimidine-H), 2.33 (s, 3H, CH₃), 2.14 (s, 6H, CH₃). IR (KBr, cm⁻¹): 3303 (NH), 2223 (CN). ESI-MS: *m/z* 371.4 (M+1); C₂₁H₁₈N₆O (370.1542).

4.1.2.3. 4-(5-(4-Bromo-2,6-dimethylphenoxy)-[1,2,4]triazolo[1,5-*a*]pyrimidin-7-ylamino)benzotrile (**5c**). White solid, yield 10%. mp: decomposed. ¹H NMR (DMSO-*d*₆, 400 MHz) δ: 10.13 (s, 1H, NH), 8.44 (s, 1H, triazole-H), 7.98 (d, 2H, *J* = 8.8 Hz, Ph-H), 7.82 (d, 2H, *J* = 8.8 Hz, Ph-H), 7.60 (s, 2H, OPh-H), 5.71 (s, 1H, pyrimidine-H), 2.18 (s, 6H, CH₃). IR (KBr, cm⁻¹): 3358 (NH), 2218 (CN). ESI-MS: *m/z* 435.4 (M+1), 437.4 (M+3); C₂₀H₁₅BrN₆O (434.0491).

4.1.2.4. 4-(5-(2,4,6-Trichlorophenoxy)-[1,2,4]triazolo[1,5-*a*]pyrimidin-7-ylamino)benzotrile (**5d**). White solid, yield 8%. mp: 258–260 °C. ¹H NMR (DMSO-*d*₆, 400 MHz) δ: 10.16 (s, 1H, NH), 8.48 (s, 1H, triazole-H), 8.13 (s, 2H, OPh-H), 7.96 (d, 2H, *J* = 8.8 Hz, Ph-H), 7.84 (d, 2H, *J* = 8.8 Hz, Ph-H), 5.91 (s, 1H, pyrimidine-H). IR (KBr, cm⁻¹): 3303 (NH), 2231 (CN). ESI-MS: *m/z* 431.3 (M+1), 433.4 (M+3), 435.3 (M+5), 437.3 (M+7); C₁₈H₉Cl₃N₆O (429.9903).

4.1.2.5. 4-(5-(2,4,6-Trifluorophenoxy)-[1,2,4]triazolo[1,5-*a*]pyrimidin-7-ylamino)benzotrile (**5e**). White solid, yield 5%. mp: 248–251 °C. ¹H NMR (DMSO-*d*₆, 400 MHz) δ: 10.85 (s, 1H, NH), 8.53 (s, 1H, triazole-H), 7.96 (s, 2H, OPh-H), 7.75 (d, 2H, *J* = 8.8 Hz, Ph-H), 7.50 (d, 2H, *J* = 8.8 Hz, Ph-H), 6.54 (s, 1H, pyrimidine-H). IR (KBr, cm⁻¹): 3434 (NH), 2229 (CN). ESI-MS: *m/z* 383.4 (M+1); C₁₈H₉F₃N₆O (382.079).

4.1.3. General procedure for the synthesis of *N*-(4-substituted-phenyl)-7-substituted phenoxy-[1,2,4]triazolo[1,5-*a*]pyrimidin-5-amines (**7a–m**) and *N*⁵-(4-substituted-phenyl)-*N*⁷-substituted-phenyl-[1,2,4]triazolo[1,5-*a*]pyrimidine-5,7-diamines (**7n, 7o**)

The appropriate substituted phenols or anilines (about 2.7 mmol) were dissolved in anhydrous DMF (15 mL) in the

presence of anhydrous K₂CO₃ (about 5.4 mmol) at room temperature followed by addition of the intermediate 5,7-dichloro-[1,2,4]triazolo[1,5-*a*]pyrimidine (**3**) (about 3 mmol). The reaction mixture was stirred at 30 °C for 6–12 h (monitored by TLC). Then some water was added to the reaction mixture. The formed solid was filtered, washed with water, and dried under vacuum to give the desired intermediates **6(a–h)**, which were used in the following step without further purification. Yields ranged from 50 to 90%.

The mixture of the corresponding intermediate **6(a–h)** (about 1.5 mmol) and 4-aminobenzotrile (about 5.25 mmol) was stirred at 150 °C for about 2 h (monitored by TLC) according to the reported method. The mixture was cooled to room temperature, diluted with DMF to get a clear solution, then concentrated with a balanced amount of silica gel in vacuo. Products were purified by column chromatography with ethyl acetate/petroleum ether (1:2) to afford 15 target compounds **7a–o**, respectively. Yields ranged from 60 to 80%.

4.1.3.1. 4-((7-(2,6-Dimethylphenoxy)-[1,2,4]triazolo[1,5-*a*]pyrimidin-5-yl)amino)benzotrile (**7a**). White solid, yield 50%. mp: 290–293 °C. ¹H NMR (DMSO-*d*₆, 400 MHz) δ: 10.14 (s, 1H, NH), 8.43 (s, 1H, triazole-H), 7.97 (d, 2H, *J* = 8.8 Hz, Ph-H), 7.81 (d, 2H, *J* = 8.8 Hz, Ph-H), 7.34 (m, 3H, OPh-H), 5.68 (s, 1H, pyrimidine-H), 2.18 (s, 6H, CH₃). IR (KBr, cm⁻¹): 3295 (NH), 2224 (CN). ESI-MS: *m/z* 375.3 (M+1); C₂₀H₁₆N₆O (356.1386).

4.1.3.2. 4-((7-(2,6-Dichlorophenoxy)-[1,2,4]triazolo[1,5-*a*]pyrimidin-5-yl)amino)benzotrile (**7b**). White solid, yield 36%. mp: 273–278 °C. ¹H NMR (DMSO-*d*₆, 400 MHz) δ: 10.22 (s, 1H, NH), 8.48 (s, 1H, triazole-H), 7.97 (d, 2H, *J* = 8.7 Hz, OPh-H), 7.86 (m, 4H, Ph-H), 7.62 (d, 1H, *J* = 8.8 Hz, OPh-H), 5.93 (s, 1H, pyrimidine-H). IR (KBr, cm⁻¹): 3431 (NH), 2224 (CN). ESI-MS: *m/z* 397.3 (M+1), 401.3 (M+5); C₁₈H₁₀Cl₂N₆O (396.0293).

4.1.3.3. 4-((7-(Mesityloxy)-[1,2,4]triazolo[1,5-*a*]pyrimidin-5-yl)amino)benzotrile (**7c**). White solid, yield 70%. mp: 255–258 °C. ¹H NMR (DMSO-*d*₆, 400 MHz) δ: 10.14 (s, 1H, NH), 8.42 (s, 1H, triazole-H), 7.98 (d, 2H, *J* = 8.8 Hz, Ph-H), 7.81 (d, 2H, *J* = 8.8 Hz, Ph-H), 7.12 (s, 2H, OPh-H), 5.69 (s, 1H, pyrimidine-H), 2.33 (s, 3H, CH₃), 2.14 (s, 6H, CH₃). ¹³C NMR (DMSO-*d*₆, 100 MHz) δ: 15.73 (–CH₃ × 2), 20.82 (–CH₃), 119.73 (–CN), Ar–C (×17): 81.85, 104.18, 119.38 (×2), 130.08 (×2), 130.63 (×2), 133.72 (×2), 137.03, 144.45, 146.33, 154.04, 155.33, 156.74, 158.44. IR (KBr, cm⁻¹): 3324 (NH), 2223 (CN). ESI-MS: *m/z* 371.4 (M+1), 393.3 (M+23); C₂₁H₁₈N₆O (370.1542).

4.1.3.4. 7-(Mesityloxy)-*N*-(4-nitrophenyl)-[1,2,4]triazolo[1,5-*a*]pyrimidin-5-amine (**7d**). White solid, yield 54%. mp: 293–297 °C. ¹H NMR (DMSO-*d*₆, 400 MHz) δ: 10.33 (s, 1H, NH), 8.45 (s, 1H, triazole-H), 8.27 (d, 2H, *J* = 8.8 Hz, Ph-H), 8.03 (d, 2H, *J* = 8.8 Hz, Ph-H), 7.13 (s, 2H, OPh-H), 5.73 (s, 1H, pyrimidine-H), 2.33 (s, 3H, CH₃), 2.14 (s, 6H, CH₃). ¹³C NMR (DMSO-*d*₆, 100 MHz) δ: 15.74 (–CH₃ × 2), 20.83 (–CH₃), Ar–C (×17): 82.08, 118.89 (×2), 125.61 (×2), 130.09 (×2), 130.65 (×2), 137.07, 141.72, 146.34, 146.54, 154.16, 155.43, 156.68, 158.31. IR (KBr, cm⁻¹): 2218 (CN), 1328 (NO₂). ESI-MS: *m/z* 391.3 (M+1); C₂₀H₁₈N₆O₃ (390.144).

4.1.3.5. *N*-(4-Chlorophenyl)-7-(mesityloxy)-[1,2,4]triazolo[1,5-*a*]pyrimidin-5-amine (**7e**). White solid, yield 62%. mp: 200–205 °C. ¹H NMR (DMSO-*d*₆, 400 MHz) δ: 9.82 (s, 1H, NH), 8.36 (s, 1H, triazole-H), 7.81 (d, 2H, *J* = 8.9 Hz, Ph-H), 7.40 (d, 2H, *J* = 8.9 Hz, Ph-H), 7.11 (s, 2H, OPh-H), 5.61 (s, 1H, pyrimidine-H), 2.32 (s, 3H, CH₃), 2.13 (s, 6H, CH₃). IR (KBr, cm⁻¹): 3305 (NH). ESI-MS: *m/z* 380.3 (M+1); C₂₀H₁₈ClN₅O (379.12).

4.1.3.6. 7-(Mesityloxy)-N-(*p*-tolyl)-[1,2,4]triazolo[1,5-*a*]pyrimidin-5-amine (**7f**). White solid, yield 68%. mp: 260–263 °C. ¹H NMR (DMSO-*d*₆, 400 MHz) δ: 9.63 (s, 1H, NH), 8.33 (s, 1H, triazole-H), 7.65 (d, 2H, *J* = 8.4 Hz, Ph-H), 7.15 (d, 2H, *J* = 8.4 Hz, Ph-H), 7.11 (s, 2H, OPh-H), 5.61 (s, 1H, pyrimidine-H), 2.32 (s, 3H, OPh-CH₃), 2.27 (s, 3H, Ph-CH₃), 2.13 (s, 6H, OPh-CH₃). ¹³C NMR (DMSO-*d*₆, 100 MHz) δ: 15.72 (–CH₃ × 2), 20.80 (–CH₃), 20.87 (–CH₃), Ar–C (×17): 81.12, 118.87 (×2), 129.59 (×2), 130.07 (×2), 130.57 (×2), 132.05, 136.84, 137.65, 146.42, 153.54, 154.94, 157.21, 158.79. IR (KBr, cm^{–1}): 3301 (NH). ESI-MS: *m/z* 360.4 (M+1), 382.5 (M+23); C₂₁H₂₁N₅O (359.1746).

4.1.3.7. 7-(Mesityloxy)-N-(4-methoxyphenyl)-[1,2,4]triazolo[1,5-*a*]pyrimidin-5-amine (**7g**). Brownish black solid, yield 32%. Decomposed (below the mp). ¹H NMR (DMSO-*d*₆, 400 MHz) δ: 9.56 (s, 1H, NH), 8.30 (s, 1H, triazole-H), 7.65 (d, 2H, *J* = 9 Hz, Ph-H), 7.11 (s, 2H, OPh-H), 6.93 (d, 2H, *J* = 9 Hz, Ph-H), 5.56 (s, 1H, pyrimidine-H), 3.74 (s, 3H, OCH₃), 2.32 (s, 3H, OPh-CH₃), 2.14 (s, 6H, OPh-CH₃). ¹³C NMR (DMSO-*d*₆, 100 MHz) δ: 15.73 (–CH₃ × 2), 20.81 (–CH₃), 55.64 (–CH₃), Ar–C (×17): 80.85, 114.39 (×2), 121.56 (×2), 130.07 (×2), 130.56 (×2), 133.22, 136.83, 146.40, 153.45, 154.88, 155.47, 157.27, 158.76. IR (KBr, cm^{–1}): 3295 (NH). ESI-MS: *m/z* 376.4 (M+1), 398.4 (M+23); C₂₁H₂₁N₅O₂ (375.1695).

4.1.3.8. 4-((7-(4-Bromo-2,6-dimethylphenoxy)-[1,2,4]triazolo[1,5-*a*]pyrimidin-5-yl)amino)benzotrile (**7h**). White solid, yield 46%. mp: 285–288 °C. ¹H NMR (DMSO-*d*₆, 400 MHz) δ: 10.11 (s, 1H, NH), 8.43 (s, 1H, triazole-H), 7.97 (d, 2H, *J* = 8.8 Hz, Ph-H), 7.82 (d, 2H, *J* = 8.8 Hz, Ph-H), 7.60 (s, 2H, OPh-H), 5.71 (s, 1H, pyrimidine-H), 2.19 (s, 6H, CH₃). ¹³C NMR (DMSO-*d*₆, 100 MHz) δ: 15.57 (–CH₃ × 2), 119.71 (–CN), Ar–C (×17): 82.08, 104.26, 119.38 (×2), 120.14, 132.62 (×2), 133.45 (×2), 133.75 (×2), 144.36, 147.77, 153.42, 155.38, 156.77, 158.35. IR (KBr, cm^{–1}): 3358 (NH), 2218 (CN). ESI-MS: *m/z* 435.6 (M+1), 437.6 (M+3); C₂₀H₁₅BrN₆O (434.0491).

4.1.3.9. 4-(((4-Cyanophenyl)amino)-[1,2,4]triazolo[1,5-*a*]pyrimidin-7-yl)oxy)-3,5-dimethylbenzotrile (**7i**). White solid, yield 60%. mp: 285–287 °C. ¹H NMR (DMSO-*d*₆, 400 MHz) δ: 10.10 (s, 1H, NH), 8.45 (s, 1H, triazole-H), 7.97 (d, 2H, *J* = 8.6 Hz, Ph-H), 7.92 (s, 2H, OPh-H), 7.82 (d, 2H, *J* = 8.6 Hz, Ph-H), 5.67 (s, 1H, pyrimidine-H), 2.23 (s, 6H, CH₃). ¹³C NMR (DMSO-*d*₆, 100 MHz) δ: 15.59 (–CH₃ × 2), 118.51 (–CN), 119.69 (–CN), Ar–C (×17): 82.31, 104.36, 110.74, 119.43 (×2), 133.03 (×2), 133.77 (×2), 134.13 (×2), 144.29, 151.82, 152.87, 155.46, 156.79, 158.27. IR (KBr, cm^{–1}): 3342 (NH), 2223 (CN). ESIMS: *m/z* 382.5 (M+1), 404.5 (M+23); C₂₁H₁₅N₇O (381.1338).

4.1.3.10. 4-(((7-(4-Chloro-2,6-dimethylphenoxy)-[1,2,4]triazolo[1,5-*a*]pyrimidin-5-yl)amino)benzotrile (**7j**). White solid, yield 52%. mp: 285–286 °C. ¹H NMR (DMSO-*d*₆, 400 MHz) δ: 10.12 (s, 1H, NH), 8.43 (s, 1H, triazole-H), 7.98 (d, 2H, *J* = 8.8 Hz, Ph-H), 7.81 (d, 2H, *J* = 8.8 Hz, Ph-H), 7.46 (s, 2H, OPh-H), 5.71 (s, 1H, pyrimidine-H), 2.19 (s, 6H, CH₃). ¹³C NMR (DMSO-*d*₆, 100 MHz) δ: 15.67 (–CH₃ × 2), 119.71 (–CN), Ar–C (×17): 82.08, 104.26, 119.38 (×2), 129.68 (×2), 131.67, 133.10 (×2), 133.74 (×2), 144.36, 147.26, 153.50, 155.38, 156.77, 158.36. IR (KBr, cm^{–1}): 3432 (NH), 2227 (CN). ESI-MS: *m/z* 391.3 (M+1), 413.5 (M+23); C₂₀H₁₅ClN₆O (390.0996).

4.1.3.11. 4-(((7-(2,4,6-Trichlorophenoxy)-[1,2,4]triazolo[1,5-*a*]pyrimidin-5-yl)amino)benzotrile (**7k**). White solid, yield 45%. mp: 246–252 °C. ¹H NMR (DMSO-*d*₆, 400 MHz) δ: 10.20 (s, 1H, NH), 8.49 (s, 1H, triazole-H), 8.13 (s, 2H, OPh-H), 7.97 (d, 2H, *J* = 8.6 Hz, Ph-H), 7.84 (d, 2H, *J* = 8.6 Hz, Ph-H), 5.93 (s, 1H, pyrimidine-H). IR (KBr, cm^{–1}): 3323 (NH), 2231 (CN). ESI-MS: *m/z* 431.2 (M+1), 433.3 (M+3), 435.3 (M+5), 437.3 (M+7); C₁₈H₉Cl₃N₆O (429.9903).

4.1.3.12. 4-(((7-(2,4,6-Tribromophenoxy)-[1,2,4]triazolo[1,5-*a*]pyrimidin-5-yl)amino)benzotrile (**7l**). White solid, yield 36%. mp: 270–273 °C. ¹H NMR (DMSO-*d*₆, 400 MHz) δ: 10.22 (s, 1H, NH), 8.49 (s, 1H, triazole-H), 8.32 (s, 2H, OPh-H), 7.98 (d, 2H, *J* = 8.7 Hz, Ph-H), 7.84 (d, 2H, *J* = 8.7 Hz, Ph-H), 5.90 (s, 1H, pyrimidine-H). IR (KBr, cm^{–1}): 3432 (NH), 2227 (CN). ESI-MS: *m/z* 563.0 (M+1), 565.1 (M+3), 357.1 (M+5), 569.0 (M+7); C₁₈H₉Br₃N₆O (561.8388).

4.1.3.13. 4-(((7-(2,6-Dibromo-4-methylphenoxy)-[1,2,4]triazolo[1,5-*a*]pyrimidin-5-yl)amino)benzotrile (**7m**). White solid, yield 46%. mp: 278–282 °C. ¹H NMR (DMSO-*d*₆, 400 MHz) δ: 10.21 (s, 1H, NH), 8.48 (s, 1H, triazole-H), 7.98 (d, 2H, *J* = 8.3 Hz, Ph-H), 7.83 (m, 4H, OPh-H, Ph-H), 5.90 (s, 1H, pyrimidine-H). ¹³C NMR (DMSO-*d*₆, 100 MHz) δ: 20.31 (–CH₃ × 2), 119.62 (–CN), Ar–C (×17): 82.60, 104.26, 116.55 (×2), 119.62 (×2), 133.80 (×2), 134.52 (×2), 141.77, 143.25, 144.07, 152.67, 155.76, 156.74, 158.07. IR (KBr, cm^{–1}): 3440 (NH), 2226 (CN). ESI-MS: *m/z* 500.9 (M+3); C₁₉H₁₂Br₂N₆O (497.9439).

4.1.3.14. 4-(((7-(Mesitylamino)-[1,2,4]triazolo[1,5-*a*]pyrimidin-5-yl)amino)benzotrile (**7n**). White solid, yield 33%. mp: 275–278 °C. ¹H NMR (DMSO-*d*₆, 400 MHz) δ: 9.79 (s, 1H, NH), 9.51 (s, 1H, NH), 8.36 (s, 1H, triazole-H), 7.97 (d, 2H, *J* = 8.8 Hz, Ph-H), 7.75 (d, 2H, *J* = 8.8 Hz, Ph-H), 7.06 (s, 2H, NPh-H), 5.21 (s, 1H, pyrimidine-H), 2.31 (s, 3H, CH₃), 2.16 (s, 6H, CH₃). ¹³C NMR (DMSO-*d*₆, 100 MHz) δ: 17.91 (–CH₃ × 2), 21.01 (–CH₃), 119.98 (–CN), Ar–C (×17): 76.74, 102.97, 118.90 (×2), 129.70 (×2), 131.54, 133.54 (×2), 136.65 (×2), 137.69, 145.39, 147.06, 154.30, 155.74, 158.24. IR (KBr, cm^{–1}): 3354 (NH), 3251 (NH), 2219 (CN). ESI-MS: *m/z* 370.4 (M+1); C₂₁H₁₉N₇ (369.1702).

4.1.3.15. 4-(((7-((2,6-Dimethylphenyl)amino)-[1,2,4]triazolo[1,5-*a*]pyrimidin-5-yl)amino)benzotrile (**7o**). White solid, yield 48%. mp: >300 °C. ¹H NMR (DMSO-*d*₆, 400 MHz) δ: 9.79 (s, 1H, NH), 9.59 (s, 1H, NH), 8.36 (s, 1H, triazole-H), 7.95 (d, 2H, *J* = 8.8 Hz, Ph-H), 7.74 (d, 2H, *J* = 8.8 Hz, Ph-H), 7.26 (m, 3H, NPh-H), 5.19 (s, 1H, pyrimidine-H), 2.20 (s, 6H, CH₃). ¹³C NMR (DMSO-*d*₆, 100 MHz) δ: 17.99 (–CH₃ × 2), 119.97 (–CN), Ar–C (×17): 76.78, 103.00, 118.92 (×2), 128.49, 129.14 (×2), 133.56 (×2), 134.17, 137.02 (×2), 145.36, 146.86, 154.33, 155.73, 158.22. IR (KBr, cm^{–1}): 3295 (NH), 3294 (NH), 2221 (CN). ESI-MS: *m/z* 356.4 (M+1), 378.5 (M+23); C₂₀H₁₇N₇ (355.1545).

4.2. *In vitro* anti-HIV assay

Evaluation of the antiviral activity of the compounds was performed using the MTT assay as previously described [27,28]. Stock solutions (10× final concentration) of test compounds were added in 25 μl volumes to two series of triplicate wells so as to allow simultaneous evaluation of their effects in mock- and HIV-infected cells. Serial 5-fold dilutions of test compounds were made directly in flat-bottomed 96-well microtiter trays using a Biomek 3000 robot (Beckman instruments, Fullerton, CA). Untreated control HIV- and mock-infected cell samples were included for each sample. HIV-1 (III_B), RES056 or HIV-2 (ROD) [24–26] stock (50 μl) at 100–300 CCID₅₀ (50% cell culture infectious dose) or culture medium was added to either the infected or mock-infected wells of the microtiter tray. Mock-infected cells were used to evaluate the effect of test compounds on uninfected cells in order to assess their cytotoxicity. Exponentially growing MT-4 cells were centrifuged for 5 min at 1000 rpm and the supernatant was discarded. The MT-4 cells were resuspended at 6 × 10⁵ cells/ml, and 50 μl volumes were transferred to the microtiter tray wells. Five days after infection, the viability of mock- and HIV-infected cells was examined spectrophotometrically by the MTT assay.

The MTT assay is based on the reduction of yellow colored 3-(4,5-dimethylthiazol-2-yl)-2,5-diphenyltetrazolium bromide (MTT) (Acros Organics, Geel, Belgium) by mitochondrial dehydrogenase of metabolically active cells to a blue-purple formazan that can be measured spectrophotometrically. The absorbances were read in an eight-channel computer-controlled photometer (Multiscan Ascent Reader, Labsystems, Helsinki, Finland), at two wavelengths (540 and 690 nm). All data were calculated using the median OD (optical density) value of two or three wells.

The 50% effective antiviral concentration (EC₅₀) was defined as the concentration of the tested compound achieving 50% protection from viral cytopathicity. The 50% cytotoxic concentration (CC₅₀) was defined as the compound concentration that reduced the viability of mock-infected cells by 50%. The symbol '>' was used to indicate the highest concentration at which the compound was tested and still found to be non-cytotoxic.

4.3. HIV-1 RT inhibition assay

Inhibition assay of HIV-1 RT_{wt} was implemented by utilizing the template/primer hybrid poly (A) × oligo (dT)₁₅, digoxigenin- and biotin-labeled nucleotides, an antibody to digoxigenin which conjugated to peroxidase (anti-DIG-POD), and the peroxidase substrate ABTS. The incorporation quantities of the digoxigenin- and biotin-labeled dUTP into DNA represented the activity of HIV-1 RT. The HIV-RT inhibition assay was performed by using an RT assay kit (Roche), and the procedure for assaying RT inhibition was performed as described in the kit protocol [30,31]. The tested compound **7i** and the control drug ETV was used at different concentration gradient (0.1 µg/ml, 1 µg/ml, 10 µg/ml, 100 µg/ml, 1 mg/ml for **7i**; 0.01 µg/ml, 0.1 µg/ml, 1 µg/ml, 10 µg/ml, 100 µg/ml, 1 mg/ml for ETV). Concretely, the reaction mixture consisted of template/primer complex, 2'-deoxy-nucleotide-5'-triphosphates (dNTPs) and reverse transcriptase (RT) enzyme in the lysis buffer with or without inhibitors. After 1 h incubation at 37 °C the reaction mixture was transferred to streptavidine-coated microtiter plate (MTP). The biotin labeled dNTPs that are incorporated in the template due to activity of RT were bound to streptavidine. The unbound dNTPs were washed using wash buffer and then antidigoxigenin-peroxidase (anti-DIG-POD) was added in MTP. The DIG-labeled dNTPs incorporated in the template was bound to anti-DIG-POD antibody. The unbound anti-DIG-POD was washed carefully by using buffer and the peroxide substrate (ABST) was added to the MTP. A colored reaction product was produced during the cleavage of the substrate catalyses by a peroxide enzyme. The absorbance of the sample was determined at OD 405 nm using microtiter plate ELISA reader. The resulting color intensity was directly proportional to the actual RT activity. The percentage inhibitory activity of RT inhibitors was calculated by comparing to a sample that does not contain an inhibitor. The percentage inhibition was calculated by formula as given below: inhibition rate % = 100 - (OD 405 nm without inhibitor - OD 405 nm with inhibitor)/(OD 405 nm without inhibitor - OD 405 nm background) × 100. IC₅₀ values corresponded to the concentration of the tested compounds required to inhibit biotin-dUTP incorporation into the HIV-1 RT by 50%.

4.4. Molecular modeling

The molecules (**5b**, **7c**, **7n** and ETV) for docking were optimized for 2000-generations until the maximum derivative of energy became 0.05 kcal/(mol*Å), using the Tripos force field. Charges were computed and added according to Gasteiger–Huckel parameters. The published three-dimensional crystal structures of wt RT complexes with ETV (PDB code: 3MEC) and double mutant RT

complexes with TMC278 (PDB code: 3BGR) were retrieved from the Protein Data Bank and were used for the docking studies by means of surflex-docking module of Sybyl-1.1. The protein was prepared by using the Biopolymer application accompanying Sybyl: The bound ligand was extracted from the complexes, water molecules were removed, hydrogen atoms were added, and charges and atom types were assigned according to AMBER99. After the protomol was generated, the optimized compounds **5b**, **7c**, **7n** and ETV were surflex-docked into the binding pocket of NNRTIs, with the relevant parameters set as defaults. The original ligand (ETV/TMC278) of the coordinates (3MEC/3BGR) was used as reference molecule to calculate the RMSD values. The docking scores related to binding affinities were calculated based on hydrophobic, polar, and repulsive interactions as well as entropic effects and solvation. Top-scoring poses were shown by the software of PyMOL version 1.5 (<http://www.pymol.org/>), in overlap with the bound ligand (ETV) in the binding site of RT. The secondary structure of RT are shown in cartoons, and only the key residues for interactions with the inhibitors were shown in sticks and labeled. The potential hydrogen-bonds were presented by dashed lines.

Conflict of interest

The authors declare no conflict of interest.

Acknowledgment

The financial support from the National Natural Science Foundation of China (NSFC No. 81273354, No. 81102320), Key Project of NSFC for International Cooperation (No. 30910103908), Research Fund for the Doctoral Program of Higher Education of China (No. 20110131130005, 20110131120037), Shandong Provincial Natural Science Foundation, China (No. ZR2009CM016), and KU Leuven (GOA 10/014) is gratefully acknowledged.

We thank K. Erven, K. Uyttersprot and C. Heens for technical assistance with the anti-HIV assays.

Appendix A. Supplementary data

Supplementary data related to this article can be found at <http://dx.doi.org/10.1016/j.ejmech.2014.07.104>. These data include MOL files and InChiKeys of the most important compounds described in this article.

References

- [1] E. De Clercq, The design of drugs for HIV and HCV, *Nat. Rev. Drug. Discov.* 6 (2007) 1001–1018.
- [2] P. Zhan, X. Liu, Novel HIV-1 non-nucleoside reverse transcriptase inhibitors: a patent review (2005–2010), *Expert Opin. Ther. Patents* 21 (2011) 717–796.
- [3] P. Zhan, X. Liu, Z. Li, Recent advances in the discovery and development of novel HIV-1 NNRTI platforms: 2006–2008 update, *Curr. Med. Chem.* 16 (2009) 2876–2889.
- [4] Y. Song, P. Zhan, X. Liu, Recent advances in the discovery and development of novel HIV-1 NNRTI platforms (Part II): 2009–2013 update, *Curr. Med. Chem.* 21 (2013) 329–355.
- [5] P. Zhan, X. Liu, Z. Li, C. Pannecouque, E. De Clercq, Design strategies of novel NNRTIs to overcome drug resistance, *Curr. Med. Chem.* 16 (2009) 3903–3917.
- [6] P. Zhan, X. Chen, D. Li, Z. Fang, E. De Clercq, X. Liu, HIV-1 NNRTIs: structural diversity, pharmacophore similarity, and implications for drug design, *Med. Res. Rev.* 33 (2013) E1–E72.
- [7] D. Li, P. Zhan, E. De Clercq, X. Liu, Strategies for the design of HIV-1 non-nucleoside reverse transcriptase inhibitors: lessons from the development of seven representative paradigms, *J. Med. Chem.* 55 (2012) 3595–3613.
- [8] P. Sax, FDA approval: etravirine, *AIDS Clin. Care* 20 (2008) 17–18.
- [9] M. Schöller-Gyüre, T.N. Kakuda, G. De Smedt, H. Vanaken, M.P. Bouche, M. Peeters, B. Woodfall, R.M. Hoetelmans, A pharmacokinetic study of etravirine (TMC125) co-administered with ranitidine and omeprazole in HIV-negative volunteers, *Br. J. Clin. Pharmacol.* 66 (2008) 508–516.

- [10] E. Seminari, A. Castagna, A. Lazzarin, Etravirine for the treatment of HIV infection, *Expert Rev. Anti-infective Ther.* 6 (2008) 427–433.
- [11] B.C. Johnson, G.T. Pauly, G. Rai, D. Patel, J.D. Bauman, H.L. Baker, K. Das, J.P. Schneider, D.J. Maloney, E. Arnold, A comparison of the ability of rilpivirine (TMC278) and selected analogues to inhibit clinically relevant HIV-1 reverse transcriptase mutants, *Retrovirology* 9 (2012) 99.
- [12] D. Li, P. Zhan, H. Liu, C. Pannecouque, J. Balzarini, E. De Clercq, X. Liu, Synthesis and biological evaluation of pyridazine derivatives as novel HIV-1 NNRTIs, *Bioorg. Med. Chem.* 21 (2013) 2128–2134.
- [13] X. Li, W. Chen, Y. Tian, H. Liu, P. Zhan, C. Pannecouque, J. Balzarini, E. De Clercq, X. Liu, Discovery of novel diarylpyrimidines as potent HIV NNRTIs via a structure-guided core-refining approach, *Eur. J. Med. Chem.* 80 (2013) 112–121.
- [14] J. Wang, P. Zhan, Z. Li, E. De Clercq, C. Pannecouque, J. Balzarini, X. Liu, Synthesis and biological evaluation of substituted nitropyridine derivatives as potent HIV-1 non-nucleoside reverse transcriptase inhibitors, *Eur. J. Med. Chem.* 76 (2013) 531–538.
- [15] A. Raney, R. Hamatake, W. Xu, J. Vernier, J. Girardet, P. Weingarten, D. Zhou, H. Kim, R. Dick, L. Yeh, RDEA427 and RDEA640 are novel NNRTIs with potent anti-HIV activity against NNRTI-resistant viruses, in: 15th Conference on Retroviruses and Opportunistic Infections (CROI), 2008, pp. 3–6.
- [16] E.H. Kerns, L. Di, *Drug-like Properties: Concepts, Structure Design and Methods: from ADME to Toxicity Optimization*, Elsevier, London, 2008.
- [17] Deepak Dalvie, Ping Kang, Cho-Ming Loi, Lance Goulet, S. Nair, Influence of heteroaromatic rings on ADME properties of drugs, in: D.A. Smith (Ed.), *Metabolism, Pharmacokinetics and Toxicity of Functional Groups: Impact of Chemical Building Blocks on ADMET*, Royal Society of Chemistry, London, 2010, pp. 328–369.
- [18] Y. Song, P. Zhan, Q. Zhang, X. Liu, Privileged scaffolds or promiscuous binders: a glance of pyrrolo [2, 1-f][1, 2, 4] triazines and related bridgehead nitrogen heterocycles in medicinal chemistry, *Curr. Pharm. Des.* 19 (2013) 1528–1548.
- [19] R. Gujjar, F. El Mazouni, K.L. White, J. White, S. Creason, D.M. Shackleford, X. Deng, W.N. Charman, I. Bathurst, J. Burrows, D.M. Floyd, D. Matthews, F.S. Buckner, S.A. Charman, M.A. Phillips, P.K. Rathod, Lead optimization of aryl and aralkyl amine-based triazolopyrimidine inhibitors of *Plasmodium falciparum* dihydroorotate dehydrogenase with antimalarial activity in mice, *J. Med. Chem.* 54 (2011) 3935–3949.
- [20] L. McKendry, Preparation of carbon-14 labeled N-(2, 6-dichloro-3-methylphenyl)-5, 7-dimethoxy [1, 2, 4] triazolo [1,5-a] pyrimidine-2-sulfonamide, *J. Label. Compd. Radiopharm.* 39 (1997) 231–240.
- [21] N. Zhang, S. Ayral-Kaloustian, T. Nguyen, J. Afragola, R. Hernandez, J. Lucas, J. Gibbons, C. Beyer, Synthesis and SAR of [1,2,4] triazolo [1,5-a] pyrimidines, a class of anticancer agents with a unique mechanism of tubulin inhibition, *J. Med. Chem.* 50 (2007) 319–327.
- [22] C.M. Richardson, D.S. Williamson, M.J. Parratt, J. Borgognoni, A.D. Cansfield, P. Dokurno, G.L. Francis, R. Howes, J.D. Moore, J.B. Murray, A. Robertson, A.E. Surgenor, C.J. Torrance, Triazolo [1,5-a] pyrimidines as novel CDK2 inhibitors: protein structure-guided design and SAR, *Bioorg. Med. Chem. Lett.* 16 (2006) 1353–1357.
- [23] Z. Zeng, Q. He, Y. Liang, X. Feng, F. Chen, E.D. Clercq, J. Balzarini, C. Pannecouque, Hybrid diarylbenzopyrimidine non-nucleoside reverse transcriptase inhibitors as promising new leads for improved anti-HIV-1 chemotherapy, *Bioorg. Med. Chem.* 18 (2010) 5039–5047.
- [24] M. Popovic, M.G. Sarngadharan, E. Read, R.C. Gallo, Detection, isolation, and continuous production of cytopathic retroviruses (HTLV-III) from patients with AIDS and pre-AIDS, *Science* 224 (1984) 497–500.
- [25] F. Barré-Sinoussi, J.-C. Chermann, F. Rey, M.T. Nugeyre, S. Chamaret, J. Gruest, C. Dautuet, C. Axler-Blin, F. Vézinet-Brun, C. Rouzioux, Isolation of a T-lymphotropic retrovirus from a patient at risk for acquired immune deficiency syndrome (AIDS), *Science* 220 (1983) 868–871.
- [26] I. Miyoshi, H. Taguchi, I. Kubonishi, S. Yoshimoto, Y. Ohtsuki, Y. Shiraishi, T. Akagi, Type C virus-producing cell lines derived from adult T cell leukemia, *Gann Monogr.* 28 (1982) 19–228.
- [27] R. Pauwels, J. Balzarini, M. Baba, R. Snoeck, D. Schols, P. Herdewijn, J. Desmyter, E. De Clercq, Rapid and automated tetrazolium-based colorimetric assay for the detection of anti-HIV compounds, *J. Virol. Methods.* 20 (1988) 309–321.
- [28] C. Pannecouque, D. Daelemans, E. De Clercq, Tetrazolium-based colorimetric assay for the detection of HIV replication inhibitors: revisited 20 years later, *Nat. Protoc.* 3 (2008) 427–434.
- [29] X.D. Ma, S.Q. Yang, S.X. Gu, Q.Q. He, F.E. Chen, E. De Clercq, J. Balzarini, C. Pannecouque, Synthesis and anti-HIV activity of aryl-2-[(4-cyanophenyl) amino]-4-pyrimidinone hydrazones as potent non-nucleoside reverse transcriptase inhibitors, *ChemMedChem* 6 (2011) 2225–2232.
- [30] K. Suzuki, B.P. Craddock, N. Okamoto, T. Kano, R.T. Steigbigel, Poly A-linked colorimetric microtiter plate assay for HIV reverse transcriptase, *J. Virol. Methods.* 44 (1993) 189–198.
- [31] Reverse Transcriptase Assay, Colorimetric kit, Roche Diagnostics GmbH, Roche. Applied Science, Sandhofer Strasse 116, D-68305 Mannheim, Germany.